Sound & Vibration 2026, 60(5), 4108.
doi: https://doi.org/10.59400/sv4108

Article

Numerical analysis of freight wagon rolling dynamics on a classification hump

Shukhrat Djabbarov*, Bakhrom Abdullayev, Aziz Gayipov, Abdusaid Yuldashov, Nodir Botir o'g'li Adilov, Irina Soboleva

Department of Wagons and Wagon Facilities, Tashkent State Transport University, Tashkent 100069, Uzbekistan; baxrom86@yandex.ru (BA); AzizG89@yandex.ru (AG); abdusaid.88.09@mail.ru (AY); adilovnodir1991@gmail.com (NBoA); irina_sobolevayu@mail.ru (IS)

*** Corresponding author:** Shukhrat Djabbarov, shuhratassistent@gmail.com

CITATION

Djabbarov S, Abdullayev B, Gayipov A, et al. Numerical analysis of freight wagon rolling dynamics on a classification hump. Sound & Vibration. 2026; 60(6): 4108. https://doi.org/10.59400/sv4108

ARTICLE INFO

Received: 28 February 2026
Revised: 28 June 2026
Accepted: 13 August 2026
Available online: 18 August 2026

Abstract: Accurate prediction of freely rolling freight-wagon speed is required to set retarder demand, maintain cut separation, and limit coupling energy in classification yards. This study develops a reproducible one-dimensional model of wagon motion along the first descending section of a classification hump. The governing equation combines the downslope gravitational component, equivalent mechanical resistance, aerodynamic drag based on signed relative air velocity, and rotating-mass inertia expressed through an effective mass. Three modelling levels are compared under identical initial conditions: gravity-only motion, constant mechanical resistance with rotating inertia, and the complete relative-wind formulation. Simulations cover a 60 m section, an initial speed of 0.50 m/s, wagon masses of 68 and 24 t, and track-aligned wind from a 12 m/s headwind to a 12 m/s tailwind. The gravity-only model overpredicts final speed by 7.8–19.7% for the loaded wagon and 3.2–41.3% for the empty wagon. For the loaded wagon, changing from headwind to tailwind raises final speed from 3.869 to 4.295 m/s and reduces travel time from 27.21 to 24.89 s. The time-stepping implementation agrees with the closed-form zero-drag solution to within 0.011%. A complete 2^4 factorial design identifies wind, gradient, and equivalent resistance as the dominant factors and reveals a substantial wind–mass interaction. A 3,500-run Monte Carlo analysis yields final-speed percentiles of 3.659, 4.074, and 4.403 m/s at P5, P50, and P95, respectively. The model is suitable for preliminary yard assessment and measurement planning; operational use requires yard-specific resistance calibration and independent field validation using separate calibration and validation datasets.

Keywords: classification hump; freight wagon; longitudinal dynamics; rolling resistance; relative wind; factorial design; uncertainty quantification

1. Introduction

A classification hump converts elevation into controlled wagon motion. The speed reached before the first retarder influences braking demand, coupling energy, and the probability that a wagon stops short. Classical yard studies and design manuals therefore treat crest conditions, profile geometry, car rollability, and retarder spacing as a connected calculation problem [1–4].

Later hump-motion studies refined the description of profile geometry and wagon kinematics [5, 6]. Even so, the resistance of a nominally identical freight car varies with load, bearings, wheel and rail condition, temperature, and local track features. Both established resistance reviews and recent on-track measurements stress the need to identify resistance from documented tests rather than assume one universal value [7,8]. A new numerical assessment of non-aerodynamic rolling resistance likewise shows why tangent- and curve-related losses must be distinguished when the track geometry requires it [9].

Aerodynamic action is usually modest at hump speeds, but it can matter for an empty wagon because force scales with relative-air-speed squared while the resulting acceleration scales inversely with mass; current freight-train aerodynamics literature also cautions that drag coefficients depend on vehicle shape and configuration [10]. At the other end of the fidelity spectrum, longitudinal-train and multibody solvers represent couplers, braking, and vehicle interactions [11,12]. International benchmark studies show that their outputs depend on connection models and numerical implementation [13,14], while network-oriented formulations trade detail for computational speed [15].

1.1. Model hierarchy and research gap

The lowest modelling level uses energy or constant-acceleration relations. It is transparent and useful for a first estimate, but it cannot explain why two wagons released at the same point roll differently. Empirical resistance equations improve the prediction, although their fitted coefficients combine several physical losses. Separating a measured wind input from an equivalent mechanical coefficient therefore offers practical value even when both are ultimately simplified.

Higher-fidelity models are indispensable when the requested output is in-train force, derailment risk, or component response. Recent work uses data-driven surrogates and monitoring systems to support such predictions [16, 17]. Heavy-haul train–track coupling research sets these longitudinal effects within a wider lateral and vertical dynamics problem [18]. Comparisons of modelling architectures and multiphysics extensions further show that model detail should be selected for the engineering decision, not added automatically [19,20].

Current implementations increasingly connect longitudinal dynamics to multibody and digital-twin environments [21, 22]. Cloud-based vehicle-dynamics simulation and scaled shunting demonstrators point toward real-time or hardware-supported validation, but they also underline the need for traceable input data and independent measurements [23,24].

The present model deliberately sits between a gravity-only estimate and those comprehensive tools. It retains a single longitudinal degree of freedom, separates track-aligned wind from equivalent mechanical resistance, includes rotating inertia, and reports uncertainty instead of one nominal speed. Earlier work by the authors supplied a hump-profile rolling formulation; the present paper narrows the claims, recasts the force balance, and adds verification and uncertainty analysis [25].

1.2. Contribution, scope, and preprint disclosure

The contribution is a reproducible workflow: assumptions and signs are stated; all variables are defined; gravity-only, constant-resistance, and relative-wind predictions are compared under identical initial conditions; the solver is checked against a closed-form limit; and factorial plus Monte Carlo analyses expose interactions and uncertainty. No claim of experimental validation is made. A preliminary version was posted on Research Square (DOI: 10.21203/rs.3.rs-8709163/v1). The article submitted in this revision has been reorganised, recalculated, and rewritten, and it should be assessed as the superseding peer-review version.

The practical research question is therefore not whether gravity accelerates a released wagon, but how much accuracy is lost when resistance, wind, and rotating inertia are omitted from an operational estimate. A hump controller must distinguish a modelling error from normal variability in wagon condition. If every discrepancy is attributed to gradient, a retarder setting may be adjusted in the wrong direction; if every discrepancy is attributed to resistance, a persistent profile-survey error can remain hidden. The present hierarchy makes those sources visible by adding one physical mechanism at a time and comparing all levels at the same release speed, distance, and loading condition. This controlled structure also clarifies the meaning of the outputs. Final speed is the state delivered to a downstream retarder model, travel time is relevant to cut separation and route timing, and translational kinetic energy provides a simple indicator of how a speed difference can amplify the energy that must subsequently be dissipated. None of these quantities alone determines impact force or structural response. Those outcomes require draft-gear, contact, and vehicle-dynamics models. By separating the low-order rolling problem from those later calculations, the workflow remains auditable and can serve as a reproducible front end for more detailed simulation rather than an attempted substitute for it.

The reduced-order position adopted here is especially useful during measurement planning. Before an expensive field campaign, the factorial experiment indicates which inputs require the tightest measurement tolerances, while the Monte Carlo calculation estimates the range of outputs created by joint input variability. The same framework can be updated after tests: surveyed gradient replaces the nominal profile, measured wind replaces the scenario value, and loading-state-specific coasting data replace the illustrative resistance range. This sequence prevents calibration from becoming an unrestricted curve-fitting exercise. Geometry and mass remain observed quantities; only parameters that genuinely represent unresolved loss mechanisms are identified. The approach also provides a clear stopping rule for model development. If the relative-wind term changes the relevant speed by less than the accepted engineering tolerance, the constant-resistance model is sufficient for that case. If the difference is material, aerodynamic inputs must be measured more carefully. If both low-order models fail against independent runs, the residual pattern can guide the addition of switch, curve, retarder, or coupling effects. In this way, complexity is introduced in response to evidence and decision sensitivity rather than by default.

2. Methodology

2.1. System boundary and assumptions

The system is one wagon, or an equivalent rigid cut, moving along the tangent of the first descending profile section. Time t and travelled distance s are independent coordinates; speed v and position s are the state variables. Positive s is downhill. The track-aligned wind component u_w is positive in the direction of wagon motion, so the relative air speed is $v - u_w$. The signed quadratic term in Equation (1) therefore reverses direction if a tailwind exceeds wagon speed. The original author schematics for the wagon, hump profile, and longitudinal force balance are restored in **Figures 1–3**.

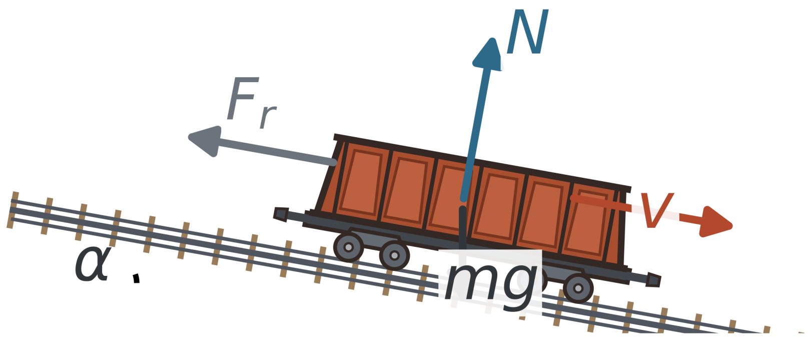

Figure 1. Forces acting on a freight wagon on an inclined track.

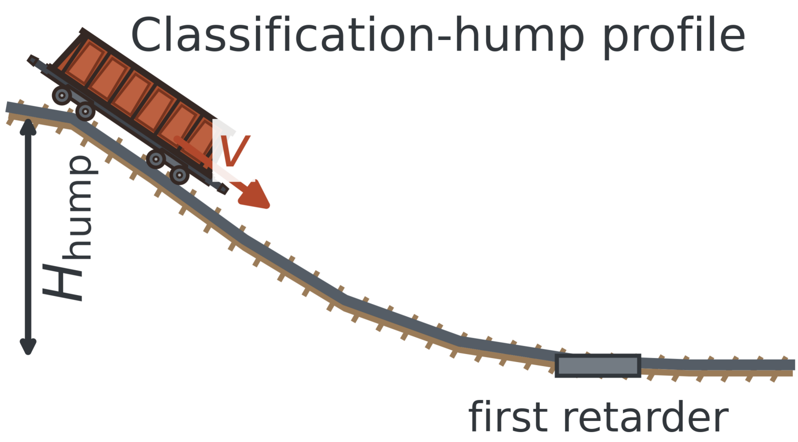

Figure 2. Classification-hump profile and wagon motion toward the first retarder.

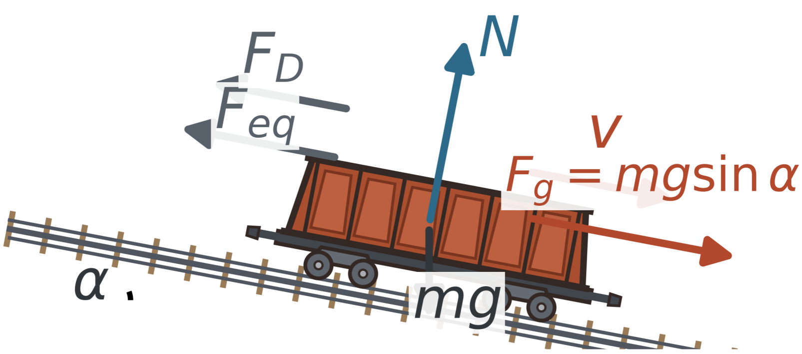

Figure 3. Longitudinal force balance during free rolling.

The calculation assumes symmetric loading, a straight track segment, no retarder action before the end point, and an equivalent representation of bearing and wheel–rail losses. It does not resolve switch geometry, curving resistance, creepage, adhesion saturation, coupler slack, draft-gear hysteresis, structural vibration, or acoustic radiation. In particular, the model makes no no-slip assertion; local contact mechanics lie outside its system boundary.

2.2. Governing equations

The complete equation set used in the calculation is given below. Equation (1) is the longitudinal force balance; Equations (2) and (3) define effective mass and equivalent mechanical resistance; Equation (4) advances position. No other force components are used in the reported simulations.

$$m_{\text{eff}}\frac{dv}{dt} = mg\sin\alpha - F_{\text{mech}} - \frac{1}{2}\rho C_D A\left(v-u_w\right)\left|v-u_w\right| \tag{1}$$

$$m_{\text{eff}} = m(1+\kappa) \tag{2}$$

$$F_{\text{mech}} = mgf_{\text{eq}}\cos\alpha \tag{3}$$

$$\frac{ds}{dt} = v \tag{4}$$

Here m is wagon mass; κ is the rotating-mass coefficient; g is gravitational acceleration; α is local slope angle; f_{eq} is the equivalent mechanical-resistance coefficient; ρ is air density; C_D is drag coefficient; A is frontal area; u_w is the wind projection along the track; v is wagon speed; s is travelled distance; and t is time. For small slopes, $\sin\alpha \approx i$ and $\cos\alpha \approx 1$, where i is the dimensionless gradient. The signed product $(v-u_w)|v-u_w|$ preserves the direction of aerodynamic force. **Table 1** summarises the input data and uncertainty ranges.

Table 1. Baseline parameters, uncertainty ranges, and identification sources.

Parameter	Symbol	Baseline	Uncertainty/Scenario range	Identification source
Profile length	L	60 m	Fixed or surveyed	Track survey/design drawing
Initial speed	v_0	0.50 m/s	0.25–0.80 m/s	Release measurement
Wagon mass	m	68,000 kg	24,000–68,000 kg	Consist or weighing data
Track gradient	i	18‰	15–21‰	Profile survey
Equivalent resistance	f_{eq}	2.5‰	1.8–4.2‰	Coasting calibration
Rotating-mass coefficient	κ	0.06	0.04–0.08	Engineering estimate
Frontal area	A	9.5 m^2	8.5–10.5 m^2	Vehicle geometry
Drag coefficient	C_D	1.20	0.90–1.40	Engineering estimate
Air density	ρ	1.225 kg/m^3	Site/temperature dependent	Meteorological data
Wind projection	u_w	0 m/s	−15 to +15 m/s	Yard anemometer
Time step	Δt	0.01 s	Step-refinement check	Numerical setting

2.3. Input data and reproducibility settings

Profile geometry and mass are measured inputs, not calibration coefficients. The equivalent resistance should be estimated from controlled coasting tests, and wind should be projected along the track. For the controlled loaded-versus-empty comparison in **Table 2**, f_{eq} is held at 2.5‰ so that the isolated mass–wind interaction can be seen. This is not an assertion that resistance is load independent: the force mgf_{eq} scales with mass, and the coefficient itself may change with axle load, bearings, temperature, and wheel–rail condition. Operational use therefore requires separate calibration by loading state. At each time step, aerodynamic force is recalculated from relative air speed, and integration ends at $s = L$.

Table 2. End-speed comparison under identical initial conditions.

Loading	Wind projection	Ideal, m/s	Constant resistance, m/s	Relative wind, m/s	Ideal deviation, %	Constant deviation, %
Loaded (68 t)	−12 m/s (headwind)	4.630	4.179	3.869	19.7	8.0
Loaded (68 t)	0 m/s	4.630	4.179	4.167	11.1	0.3
Loaded (68 t)	+12 m/s (tailwind)	4.630	4.179	4.295	7.8	−2.7
Empty (24 t)	−12 m/s (headwind)	4.630	4.179	3.277	41.3	27.5
Empty (24 t)	0 m/s	4.630	4.179	4.145	11.7	0.8
Empty (24 t)	+12 m/s (tailwind)	4.630	4.179	4.488	3.2	−6.9

2.4. Numerical solution

Equations (1) and (4) are advanced with an explicit time step. The reported simulations use $\Delta t = 0.01$ s; time-step adequacy is checked against the analytical limiting case in Equation (5). A time-domain solution also avoids division by v near release. Position, speed, acceleration, elapsed time, and translational kinetic energy are retained for post-processing.

2.5. Numerical verification and validation status

When $C_D = 0$ and i, f_{eq}, and κ are constant, Equation (1) reduces to the closed-form expression in Equation (5). For the baseline case, that expression gives $v(L) = 4.178968$ m/s, whereas the time-stepping solution gives 4.179444 m/s. The relative difference is 0.011%. This is a code-verification test only: it shows that the numerical procedure solves the stated equations in a limiting case, not that the equations reproduce a particular yard.

$$v(L) = \sqrt{v_0^2 + \frac{2g\left(i - f_{\text{eq}}\right)}{1+\kappa} L} \tag{5}$$

No traceable measured speed dataset was available for the present article. The earlier wording about agreement with “physical observations” has therefore been removed, and no observed–simulated error table is claimed. The evidence reported here is limited to (i) analytical verification, (ii) comparison among three model levels, and (iii) an engineering plausibility check against published resistance ranges. Independent validation remains future work. It should use separate calibration and validation runs and report bias, mean absolute error, root-mean-square error, and prediction-interval coverage.

2.6. Sensitivity and uncertainty design

Three analyses are used. First, a model hierarchy compares gravity-only, constant-resistance, and relative-wind predictions. Second, a complete 2^4 factorial design estimates main effects and all pairwise interactions. Third, Monte Carlo sampling propagates uncertainty in mass, gradient, equivalent resistance, wind, drag coefficient, frontal area, rotating-mass coefficient, and release speed. The outputs are final speed, travel time, and translational kinetic energy.

The force balance is evaluated with one consistent sign convention. Downhill gravity is positive. Equivalent mechanical resistance always opposes positive wagon motion and is therefore subtracted. Aerodynamic force is based on the velocity of the wagon relative to the air, not on wagon speed alone. A headwind has a negative track-aligned wind component, increases relative speed, and produces a negative drag contribution. A tailwind reduces relative speed; when it exceeds wagon speed, the signed quadratic expression becomes negative before the leading minus sign and consequently acts downhill. This treatment avoids an artificial discontinuity at equal wagon and wind speeds. The rotating-mass coefficient does not create a separate external force. Instead, it increases effective inertia, so the same net longitudinal force produces a smaller acceleration. The formulation therefore conserves the intended distinction between external forces and stored rotational kinetic energy. At the low speeds studied, air density, drag coefficient, and frontal area are held constant within each run, whereas relative air speed is recalculated at every time step.

Dimensional consistency provides a preliminary check on implementation. Each term in the numerator of the acceleration equation has units of newtons: the gravity and equivalent-resistance terms contain mass times gravitational acceleration, and the aerodynamic term contains density times area times squared speed. Division by effective mass yields metres per second squared. The position equation then advances distance in metres. Input gradients expressed in per mille are converted to dimensionless ratios before use, and wagon masses stated in tonnes are converted to kilograms. Wind signs are assigned only after projection onto the track direction. These conversions are important because a silent use of 18 rather than 0.018 for gradient, or 68 rather than 68,000 for mass, would dominate every other modelling choice. Automated checks reject non-positive mass, negative frontal area, a non-positive time step, and a profile length shorter than the current position. Scenario labels are generated from the numerical wind sign so that headwind and tailwind cannot be interchanged during post-processing.

The numerical workflow proceeds from parameter validation to state integration and then to event interpolation. At the start of a run, position is zero and speed equals the prescribed release value. The solver evaluates acceleration from the current state, updates speed, and advances position over the time step. Because the final step normally crosses the specified distance, the reported end state is linearly interpolated between the last two states rather than taken from the first point beyond the boundary. This removes a step-size-dependent distance overshoot. A run terminates if the wagon reaches the end point, and it is flagged as a non-arrival if speed falls to zero before that event. Full histories are retained so that final values can be traced back to the calculated acceleration sequence. The analytical zero-drag case is evaluated with the same inputs and endpoint. Agreement at that limit tests unit conversion, effective mass, resistance sign, integration, and endpoint handling together; it does not test whether the selected coefficients describe a physical yard.

Uncertainty propagation is separated from deterministic model comparison. The hierarchy comparison changes equations while holding inputs fixed, thereby measuring structural consequences of model choice. The factorial experiment keeps the complete equation set and changes four operationally interpretable factors at low and high levels. Coding each factor as minus one or plus one permits main effects to be calculated as differences between the corresponding group means; pairwise interactions measure how the effect of one factor changes across the level of another. Monte

Carlo sampling addresses a different question: the distribution of output when several uncertain inputs vary simultaneously. Each draw defines one internally complete wagon and environment scenario, and all reported percentiles are empirical quantiles of the resulting outputs. Rank correlation is used because the input-output relationships need not be exactly linear. The selected distributions are intentionally transparent and bounded, but they are not presented as estimates of frequencies at a named yard. Replacing them with site records is a necessary step before probabilistic operational limits are established.

3. Results

Every scenario uses a 60 m section and an initial speed of 0.50 m/s. The three model levels are (i) ideal gravity-only motion, (ii) constant mechanical resistance with a rotating-mass correction, and (iii) the relative-wind formulation. Their comparison is meant to identify when an added term changes the decision materially; it is not a presumption that the most detailed alternative is always best.

3.1. Quantitative comparison with simpler models

Figure 4 compares the three modelling levels.

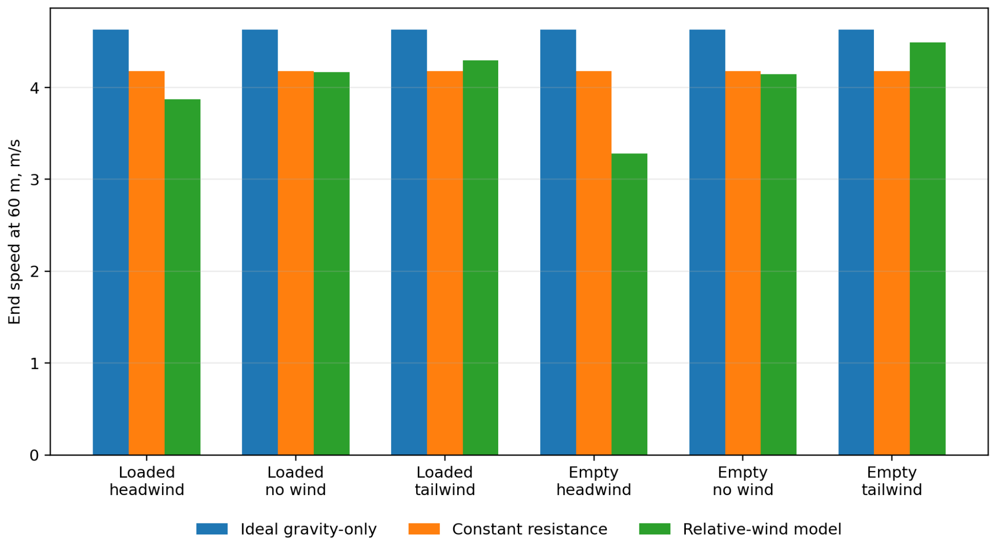

Figure 4. End-speed comparison for three modelling levels.

The ideal relation gives the largest speed because it omits dissipation and rotating inertia. For the 68 t wagon, its overprediction is 7.8% with a 12 m/s tailwind and 19.7% with a 12 m/s headwind. For the 24 t wagon, the corresponding range is 3.2–41.3%. Around the calm loaded case, constant resistance and relative wind differ by less than 1%. With an empty wagon in a 12 m/s headwind, however, constant resistance overpredicts final speed by 27.5%. Aerodynamic detail is therefore consequential mainly when the wagon is light or the track-aligned wind is strong.

3.2. Velocity–time histories and energy metrics

The original author plots for distance- and time-domain velocity histories are restored in **Figures 5** and **6**. For the loaded wagon, moving from a 12 m/s headwind to a 12 m/s tailwind increases final speed from 3.869 to 4.295 m/s and shortens travel time from 27.21 to 24.89 s. Translational kinetic energy rises from 0.509 to 0.627 MJ. Because energy depends on v^2, the 11.0% speed change corresponds to an energy increase of about 23%. These are kinematic and energy indicators only; they are not predictions of coupler force, wagon-body vibration, or noise.

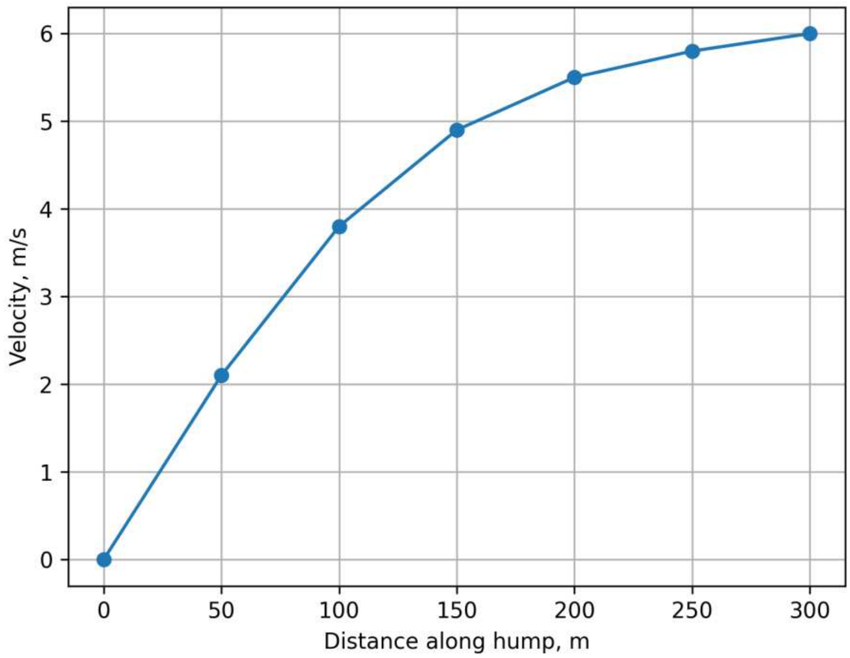

Figure 5. Velocity variation along hump distance (original author plot).

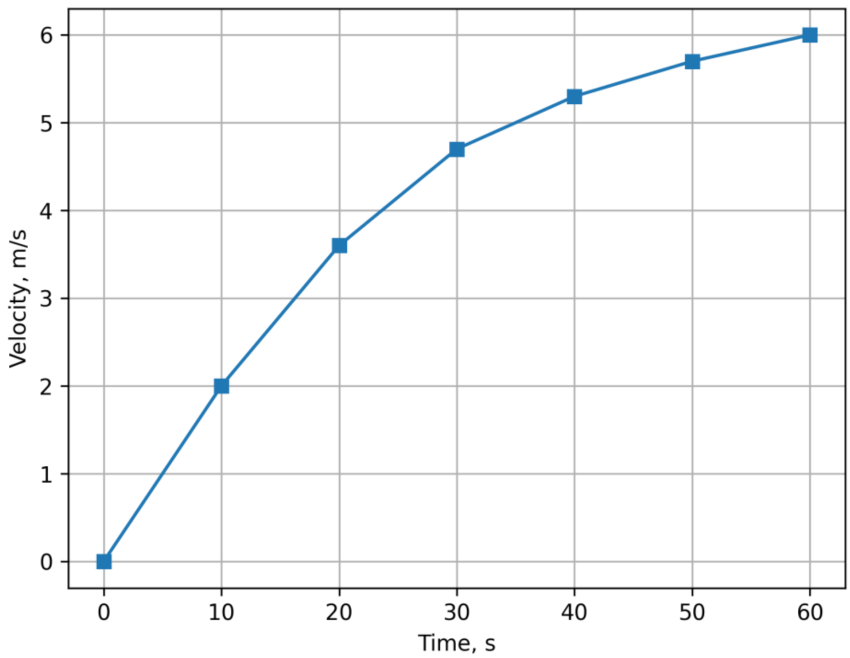

Figure 6. Velocity variation over time during wagon rolling (original author plot).

3.3. Multi-parameter sensitivity and interactions

Figure 7 presents the main and pairwise factorial effects; **Table 3** lists the largest numerical effects.

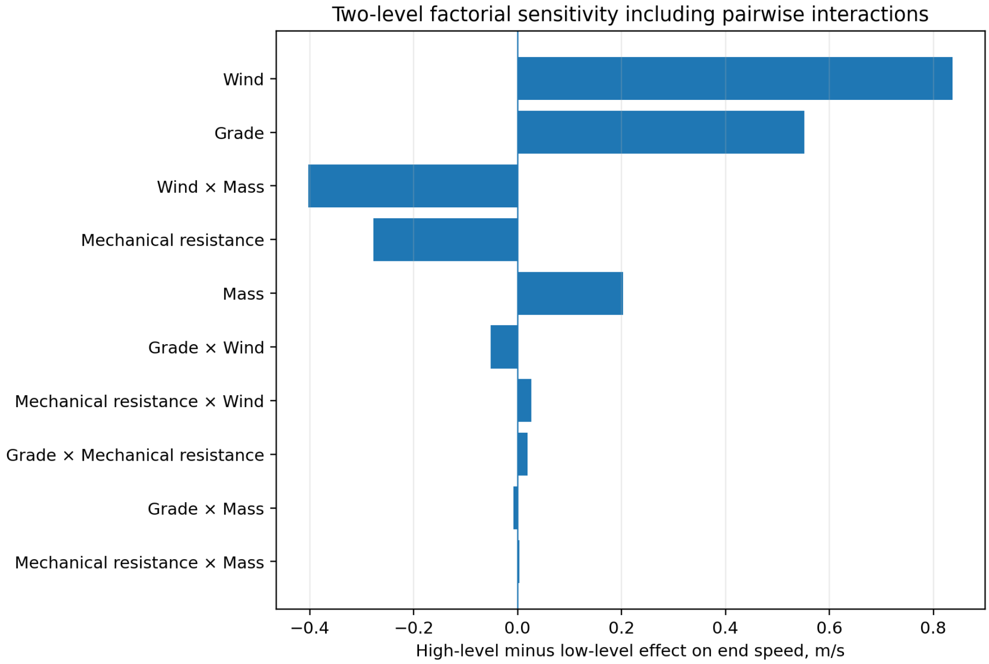

Figure 7. Main and pairwise factorial effects on end speed.

Table 3. Largest effects in the 2^4 factorial design.

Factor or interaction	High-level minus low-level effect, m/s
Wind	0.837
Grade	0.552
Wind × Mass	−0.403
Mechanical resistance	−0.277
Mass	0.203
Grade × Wind	−0.052
Mechanical resistance × Wind	0.026

The factorial levels are gradient 16–20‰, equivalent resistance 2–4‰, wind from 12 m/s headwind to 12 m/s tailwind, and wagon mass 24–68 t. They are transparent scenario bounds within **Table 1**, not an arbitrary ±20% one-factor-at-a-time perturbation and not field-derived probability limits. Wind has the largest main effect over this domain (+0.837 m/s), followed by gradient (+0.552 m/s) and resistance (−0.277 m/s). The wind × mass interaction is −0.403 m/s, confirming that the empty wagon is substantially more sensitive to wind. The remaining pairwise interactions are small for the selected domain.

3.4. Response surface and probabilistic uncertainty

Figure 8 presents the response surface, **Figure 9** shows the Monte Carlo distribution, and **Table 4** lists the corresponding percentiles.

The gradient–resistance response surface also shows an identifiability problem: different combinations can produce nearly the same final speed, so speed observations alone cannot reliably distinguish a profile error from a resistance error. Independent profile survey is essential. Across 3,500 Monte Carlo runs, final-speed percentiles are 3.659 m/s (P5), 4.074 m/s (P50), and 4.403 m/s (P95). The corresponding travel-time percentiles are 24.14, 26.14, and 28.89 s, and the kinetic-energy percentiles are 0.205, 0.376, and 0.571 MJ. The assumed distributions are illustrative; yard-specific distributions are required before setting operational risk limits.

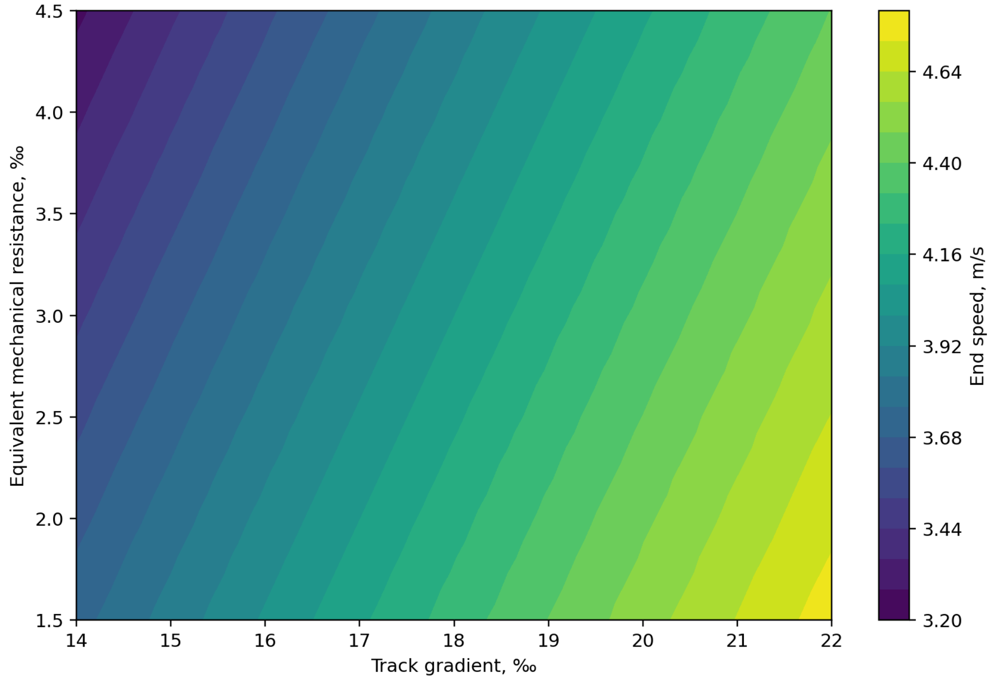

Figure 8. Response surface for gradient and equivalent mechanical resistance.

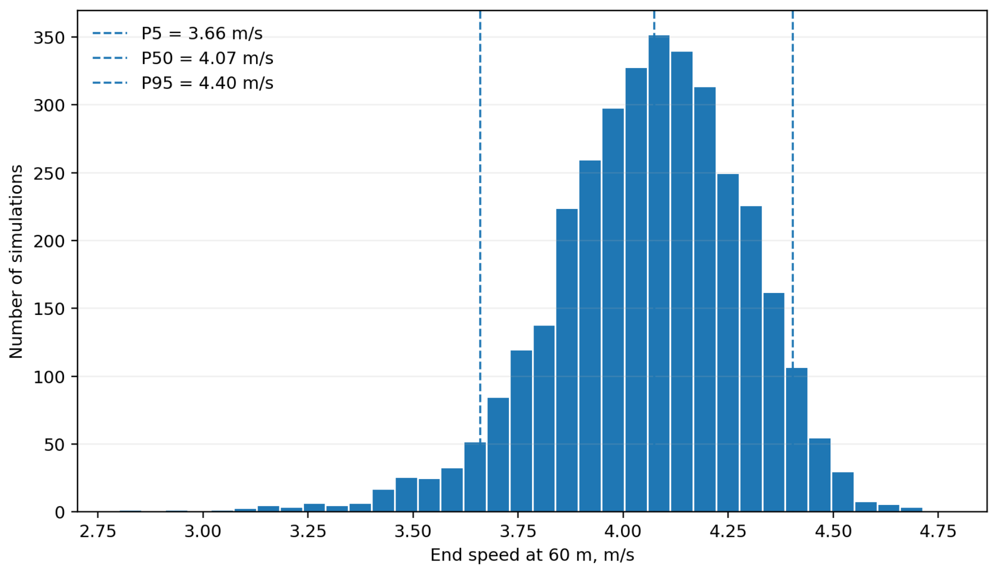

Figure 9. Monte Carlo distribution of end speed for 3,500 parameter sets.

Table 4. Monte Carlo percentile intervals.

Output	P5	P50	P95
End speed, m/s	3.659	4.074	4.403
Travel time, s	24.14	26.14	28.89
End kinetic energy, MJ	0.205	0.376	0.571

Rank correlation offers a second view of sensitivity. Gradient is most strongly associated with final speed (Spearman ρ = 0.738), followed by wind (ρ = 0.503) and resistance (ρ = −0.275). The rotating-mass coefficient has a smaller negative association. Mass, frontal area, and drag coefficient have modest marginal correlations because their effects are conditional, especially through wind × mass. A single one-factor derivative would obscure that interaction.

The hierarchy comparison provides more information than a single percentage error. The gap between gravity-only and constant-resistance predictions quantifies the combined influence of mechanical loss and rotating inertia. The additional gap between constant-resistance and relative-wind predictions isolates the consequence of calculating aerodynamic force from the current relative speed. For the loaded calm-air case, this second gap is small because aerodynamic acceleration is modest compared with the gravity and resistance terms. Under headwind, the relative-speed squared term grows rapidly, and division by the lower empty-wagon mass magnifies its effect on acceleration. Under tailwind, reduced relative speed can make the aerodynamic correction small or supportive during early motion. Thus, the ordering of model predictions is not fixed by model complexity alone; it follows from the signs and magnitudes of the physical terms. Reporting both loading states prevents a conclusion derived from the loaded wagon from being applied incorrectly to an empty wagon.

The distance- and time-domain histories answer complementary questions. A speed-versus-distance curve is convenient for locating where acceleration is strongest and for passing the calculated state to equipment installed at a known chainage. A speed-versus-time curve is necessary for cut-spacing analysis and for synchronising the wagon state with route-setting or retarder commands. The curves are nonlinear because aerodynamic force changes with speed even though gradient and the equivalent resistance coefficient are constant in the example. Early in the run, gravity dominates and the wind cases remain relatively close. As speed increases, relative-air-speed differences accumulate, separating the arrival speeds and times. This accumulated effect explains why a force that appears modest instantaneously can become relevant over the full profile section. It also shows why applying one constant acceleration over the entire length can reproduce neither the detailed time history nor the correct wind dependence.

The factorial and Monte Carlo results should be read together. The factorial effects are conditional differences across deliberately wide scenario endpoints and are useful for ranking mechanisms and detecting interactions. They are not probabilities. The Monte Carlo percentiles, by contrast, depend on the assumed input distributions and describe the simulated ensemble rather than universal safety limits. Gradient has the strongest rank correlation because it acts continuously through the gravity term across every sampled case. Wind remains highly influential, but its marginal correlation is moderated by mass and by the nonlinear relative-speed term. The negative resistance correlation agrees with the force balance, while the smaller correlations for drag coefficient and frontal area do not imply that those parameters are physically irrelevant. Their influence is most visible in combinations that also produce large relative wind. The strong wind–mass interaction in the factorial design supplies the evidence that a purely marginal ranking would otherwise conceal.

4. Discussion

4.1. Operational interpretation

The calculations suggest a two-timescale operating strategy. Wind can be measured continuously and used as a current input. Equivalent mechanical resistance changes more slowly and should be updated from coasting trials and maintenance evidence. Pairing a live wind measurement with loading-state-specific, seasonally calibrated resistance is more defensible than applying one speed correction throughout the year.

The model can also define conservative scenario envelopes. A tailwind together with low resistance produces the highest speed and retarder-energy demand. A headwind together with high resistance produces the greatest risk of low arrival speed or premature stopping. These are different operational hazards and should not be collapsed into a single "worst case".

The calculation can be implemented in a spreadsheet or embedded in a yard decision-support tool. Its proper output is a speed and uncertainty envelope at fixed track locations. Detailed retarder-contact, coupler-impact, vibration, or noise prediction requires a separate higher-fidelity model using the calculated speed history as an input.

4.2. Relationship to existing modelling levels

Model choice should be conditional. For a loaded wagon in calm air, constant resistance and relative wind differ by less than 1%, and the simpler calculation is adequate. For an empty wagon in a strong headwind, the difference is operationally material. The appropriate sequence is therefore to begin with a verified low-order model and add terms only when their expected contribution matters for the decision. This follows the broader lesson from longitudinal-dynamics benchmarking [13, 14]. Recent model-integration studies point in the same direction [11,19,21].

Recent hump-specific work on calculated runners and whole-profile wagon kinematics provides context for parameter selection and the relationship between local and profile-wide calculations [26, 27]. At broader scales, network-level freight simulation and a recent freight-aerodynamics review show how resistance fidelity and model scope should be matched to the decision [28, 29]. Complementary work on drag-reduction design and longitudinal-dynamics digital twins further illustrates the transition from low-order speed prediction to richer train-level analyses [30,31].

4.3. Applicability and limitations

The formulation is deliberately reduced order. The coefficient f_{eq} can absorb bearing, wheel–rail, switch, contamination, and temperature effects and is therefore not unique. Holding it constant between the 24 t and 68 t cases isolates mass and wind; it must not be interpreted as evidence of load independence. The aerodynamic term uses one C_D and one frontal area and does not resolve shielding in a wagon cut. The model also excludes lateral motion, local adhesion saturation, creepage, longitudinal slack, retarder contact, and structural response. It neither derives nor relies on a no-slip condition. Results are conditional on the 60 m profile and stated ranges and cannot be transferred to another yard without measurement and independent validation.

4.4. Field-validation protocol

A minimum field campaign should cover at least two loading states and calm, headwind, and tailwind cases. Initial and downstream speeds should be recorded at fixed surveyed positions by calibrated radar, lidar, axle-counter timing, or validated video tracking. Each run should document wagon identity, loading, wheel and bearing condition, temperature, release speed, and track-aligned wind. Only a subset should be used to identify f_{eq}; the remaining runs should be kept blind for validation. A measured-versus-predicted table and plots should then report bias, MAE, RMSE, and interval coverage. Such data are not available in this study and have not been invented.

For operational use, the numerical results must be converted into decision thresholds defined by the yard operator. A model difference is material only relative to allowable arrival-speed error, available retarder capacity, coupling-speed limits, and the required spacing between successive cuts. The present calculations do not prescribe those thresholds because they depend on yard equipment and rules. They do show how to evaluate them: calculate the same scenario with the accepted baseline model and the candidate refinement, compare speed, time, and energy at the controlled location, and retain the refinement when the difference exceeds the documented tolerance. Uncertainty intervals should then be compared with the permitted operating window. If the interval crosses a limit, the appropriate response may be a new measurement, a conservative operating rule, or a higher-fidelity calculation. Selecting only the median prediction would conceal this risk. Conversely, treating the illustrative P5–P95 range as a validated safety envelope would overstate the evidence.

A defensible calibration strategy begins with independent measurements rather than simultaneous adjustment of every parameter. Surveyed profile geometry should be fixed first. Wagon mass and release speed should be measured for each run, and wind should be recorded close to the track at a sampling rate adequate to represent the traversal period. Equivalent mechanical resistance can then be estimated from a calibration subset, preferably stratified by loading state, season, and relevant maintenance condition. Drag coefficient should not be tuned freely to compensate for unknown mechanical resistance; it should be supported by geometry-specific literature, coast-down evidence, or a separate aerodynamic assessment. Parameter estimates must be applied unchanged to the blind validation subset. Residuals should be examined against wind, mass, speed, and position because a small average error can coexist with systematic bias in empty-wagon or headwind cases. This procedure creates a traceable distinction between calibration fit and predictive performance.

Transferability is intentionally restricted. A coefficient obtained on one hump section may include local switch losses, curvature, rail condition, and temperature effects that do not persist elsewhere. Likewise, one frontal area and drag coefficient cannot represent every wagon body or shielding arrangement in a cut. Application to another site therefore requires a new profile survey, a review of wagon types, and at least a limited coasting programme. Application to coupled cuts requires additional longitudinal degrees of freedom and connection models, because internal forces and slack action can alter individual wagon histories. Wet or contaminated rail, active retarders, and very low-speed contact behaviour may also require mechanisms absent from the current equations. These limitations do not negate the value of the model within its stated domain; they define the evidence needed to extend that domain responsibly and prevent a screening calculation from being mistaken for a universally calibrated operational simulator.

The reported numerical evidence comprises three distinct datasets. **Table 2** contains eighteen deterministic endpoint predictions: two masses, three wind states, and three model levels. The factorial dataset contains all sixteen combinations of four two-level factors, allowing four main effects and six pairwise interactions to be estimated without the confounding created by one-factor-at-a-time perturbations. The probabilistic dataset contains 3,500 independently sampled parameter vectors and produces empirical distributions of speed, time, and kinetic energy. These datasets answer different questions and are not pooled. Verification uses the zero-drag limiting case, for which the analytical endpoint is 4.178968 m/s and the numerical endpoint is 4.179444 m/s; the absolute difference is 0.000476 m/s and the relative difference is approximately 0.011%. Model-form comparison uses the complete scenario matrix, whereas uncertainty analysis uses percentiles and rank correlations. This separation prevents numerical discretisation error, structural model differences, and input uncertainty from being reported as one undifferentiated error term. Experimental prediction error remains unquantified because no independent field dataset is available.

5. Conclusion

1. The governing mechanics are classical. The contribution is a transparent and bounded calculation workflow for the first hump section, not a new theory of railway motion.
2. On the 60 m example, gravity-only motion overpredicts final speed by 7.8–19.7% for a 68 t wagon and 3.2–41.3% for a 24 t wagon. The constant-resistance model is close in calm air but is 27.5% high for the empty-wagon headwind case.
3. For the loaded wagon, changing from a 12 m/s headwind to a 12 m/s tailwind raises final speed from 3.869 to 4.295 m/s and translational kinetic energy from 0.509 to 0.627 MJ. These quantities do not directly predict impact force, vibration, or sound.
4. Over the stated factorial ranges, wind, gradient, and equivalent resistance are the dominant factors. The wind × mass interaction is substantial; resistance must nevertheless be calibrated separately by loading state before operational application.
5. The analytical limiting case and numerical solution differ by about 0.011%. No field-validation dataset is reported. Instrumented trials with separate calibration and validation subsets remain necessary.
6. The model is suited to screening scenarios, prioritising measurements, and supplying speed histories to retarder, coupler-impact, or multibody analyses. It should not be used beyond its stated domain without additional terms and yard-specific validation.

Author contributions: SD conceived the study, developed the methodology, performed the principal analysis, and drafted the manuscript. BA, AG, and AY

contributed to model formulation, engineering interpretation, and critical revision. NBoA contributed to numerical implementation, data processing, and figure preparation. IS supervised the study and critically revised the manuscript. All authors reviewed and approved the final manuscript.

Funding: The authors received no specific funding for this work.

Institutional review board statement: Not applicable. This study did not involve human participants or animals.

Informed consent statement: Not applicable.

Data availability statement: The input table and numerical outputs required to reproduce the reported cases are contained in this article. Machine-readable calculation files are available from the corresponding author on reasonable request.

Acknowledgment: The authors express their gratitude to Professor Kh. T. Turanov for scientific discussions concerning classification-hump mechanics and wagon rolling calculations.

Conflict of interest: The authors declare that they have no competing interests.

AI use statement: During manuscript preparation and revision, the authors used OpenAI ChatGPT to refine English expression, improve document structure, and check reference formatting. The physical model, parameter values, numerical calculations, figures, tables, and scientific conclusions were developed or independently verified by the authors. AI was not used to generate or alter the reported numerical data. All AI-assisted output was critically reviewed and edited, and the authors accept full responsibility for the content.

References

1. Stock WA, Sakasita M, Elliott CV, et al. PROFILE: Gradient simulation for rail hump classification yards. Transportation Research Record. 1980; (744): 52–58.
2. Petracek SJ, Savage NP. Freight Car Rollability: Task 1—Review and Requirements. US Department of Transportation; 1980.
3. Wong PJ. Railroad Classification Yard Technology Manual. Vol. III: Freight Car Rolling Resistance. US Department of Transportation; 1981.
4. Kozachenko D, Bobrovskyi V, Demchenko Y. A method for optimization of time intervals between rolling cuts on sorting humps. Journal of Modern Transportation. 2018; 26(3): 189–199. doi: 10.1007/s40534-018-0161-2
5. Saidivaliev SU. Determining the kinematic parameters of railcar motion in hump yard retarder positions. AIP Conference Proceedings. 2023; 2612: 060016. doi: 10.1063/5.0115115
6. Turanov K, Gordienko A, Saidivaliev S, et al. Designing the height of the first profile of the marshalling hump. E3S Web of Conferences. 2020; 164: 03038. doi: 10.1051/e3sconf/202016403038
7. Michálek T, Kohout M, Šlapák J, et al. Curving and running resistance of freight trains: current experience with on-track measurements. Vehicle System Dynamics. 2025; 63: 1983–1997. doi: 10.1080/00423114.2024.2398003
8. Rochard BP, Schmid F. A review of methods to measure and calculate train resistances. Proceedings of the Institution of Mechanical Engineers, Part F: Journal of Rail and Rapid Transit. 2000; 214(4): 185–199. doi: 10.1243/0954409001531306
9. Wu Q, Ahmad S, Spiryagin M, et al. A method to numerically assess rail vehicle rolling resistance on tangent and curved tracks. Vehicle System Dynamics. 2026. doi: 10.1080/00423114.2026.2615792
10. Wu Q, Li T, Cole C, et al. A review of air drag related freight train aerodynamics. Part 1: Assessment methods.

Heavy Rail. 2026; 2: 100002. doi: 10.1016/j.hrail.2026.100002
11. Magelli M, Zampieri N. A novel approach for longitudinal train dynamics simulations with multibody codes. Vehicle System Dynamics. 2025; 63(5): 978–996. doi: 10.1080/00423114.2024.2362949
12. Bosso N, Magelli M, Zampieri N. Validation of a new longitudinal train dynamics code for time-domain simulations and modal analyses. International Journal of Transport Development and Integration. 2021; 5(1): 41–56. doi: 10.2495/TDI-V5-N1-41-56
13. Spiryagin M, Wu Q, Cole C. International benchmarking of longitudinal train dynamics simulators: Benchmarking questions. Vehicle System Dynamics. 2017; 55(4): 450–463. doi: 10.1080/00423114.2016.1270457
14. Wu Q, Spiryagin M, Cole C, et al. International benchmarking of longitudinal train dynamics simulators: Results. Vehicle System Dynamics. 2018; 56(3): 343–365. doi: 10.1080/00423114.2017.1377840
15. Wang J, Rakha HA. Longitudinal train dynamics model for a rail transit simulation system. Transportation Research Part C: Emerging Technologies. 2018; 86: 111–123. doi: 10.1016/j.trc.2017.10.011
16. Bosso N, Magelli M, Trinchero R, et al. Application of machine learning techniques to build digital twins for long train dynamics simulations. Vehicle System Dynamics. 2024; 62(1): 21–40. doi: 10.1080/00423114.2023.2174885
17. Zhang S, Huang P, Yan W. A data-driven approach for railway in-train forces monitoring. Advances in Engineering Informatics. 2024; 59: 102258. doi: 10.1016/j.aei.2023.102258
18. Zhai W, Stichel S, Ling L. Train–track coupled dynamics problems in heavy-haul rail transportation. Vehicle System Dynamics. 2025; 63(7): 1187–1240. doi: 10.1080/00423114.2025.2494834
19. Magelli M, Corrêa PHA, Santos AA. Assessing the effect of modelling approaches for longitudinal train dynamics simulations with a multibody code. Proceedings of the Institution of Mechanical Engineers, Part K: Journal of Multi-body Dynamics. 2025; 239(4): 326–338. doi: 10.1177/14644193251368540
20. Magelli M, Zampieri N, Wu Q. Integration of brake-block thermal equations within a railway-vehicle multibody model: a multiphysics approach. International Journal of Rail Transportation. 2025; 13(1): 69–84. doi: 10.1080/23248378.2023.2301618
21. Bosso N, Gugliotta A, Magelli M, et al. Integrating longitudinal train dynamics simulations within multibody models. CIVIL-COMP Conference. 2024; 7: 1–11. doi: 10.4203/ccc.7.5.12
22. Bernal E, Wu Q, Spiryagin M, et al. Augmented digital twin for railway systems. Vehicle System Dynamics. 2024; 62(1): 67–83. doi: https://doi.org/10.1080/00423114.2023.2194543
23. Tang Z, Ling L, Zhang T, et al. Towards digital twin trains: implementing a cloud-based framework for railway vehicle dynamics simulation. International Journal of Rail Transportation. 2025; 13(3): 444–467. doi: 10.1080/23248378.2024.2355578
24. Hofmeier T, Cichon M. Introducing scaled model development to on-sight automatic train operation. In: Proceedings of the 10th International Conference on Vehicle Technology and Intelligent Transport Systems; 2–4 May 2024; Angers, France. doi: 10.5220/0012691500003702
25. Djabbarov S, Saidivaliev S, Abdullaev B, et al. Mathematical model of wagon wheels rolling along the hump profile. E3S Web of Conferences. 2023; 460: 06007. doi: 10.1051/e3sconf/202346006007
26. Djabbarov S, Abdullaev B. Updating the parameters of the “calculated runners” used in the design of sorting slides. AIP Conference Proceedings. 2026; 3374: 050024. doi: 10.1063/5.0317222
27. Turanov K, Gordienko A, Saidivaliev S, et al. Kinematic characteristics of the car movement from the top to the calculation point of the marshalling hump. In: Murgul V, Pukhkal V (editors). Advances in Intelligent Systems and Computing. Springer; 2021. doi: 10.1007/978-3-030-57450-5_29
28. Aredah AS, Fadhloun K, Rakha HA. NeTrainSim: A network-level simulator for modeling freight train longitudinal motion and energy consumption. Railway Engineering Science. 2024; 32: 480–498. doi: 10.1007/s40534-024-00331-x
29. Corniani L, Schito P, Bell J, et al. A review of freight train aerodynamics. Proceedings of the Institution of Mechanical Engineers, Part F: Journal of Rail and Rapid Transit. 2026; 240(2): 133–150. doi: 10.1177/09544097251382265
30. Wu Q, Li T, Cole C, et al. A review of air drag related freight train aerodynamics. Part 2: Energy efficient designs. Heavy Rail. 2026; 2: 100003. doi: 10.1016/j.hrail.2026.100003
31. Bosso N, Cantone L, Gugliotta A, et al. Introduction of digital twins in the longitudinal train dynamics simulation of freight train air brake operations. In: Huang W, Ahmadian M (editors). Advances in Dynamics of Vehicles on Roads and Tracks III. Springer; 2025. pp. 297–306. doi: 10.1007/978-3-031-66971-2_32